Published in final edited form as:
J Magn Reson. 2014 April ; 241: 18–31. doi:10.1016/j.jmr.2014.01.005.

Sensitivity Enhancement in Solution NMR: Emerging Ideas and New Frontiers

Jung Ho Lee, **Yusuke Okuno**, and **Silvia Cavagnero***
Department of Chemistry and Biophysics Program, University of Wisconsin-Madison, 1101 University Avenue, Madison, Wisconsin 53706-1322, USA

Abstract

Modern NMR spectroscopy has reached an unprecedented level of sophistication in the determination of biomolecular structure and dynamics at atomic resolution in liquids. However, the sensitivity of this technique is still too low to solve a variety of cutting-edge biological problems in solution, especially those that involve viscous samples, very large biomolecules or aggregation-prone systems that need to be kept at low concentration. Despite the challenges, a variety of efforts have been carried out over the years to increase sensitivity of NMR spectroscopy in liquids. This review discusses basic concepts, recent developments and future opportunities in this exciting area of research.

Keywords

NMR Sensitivity; Hyperpolarization; Dissolution DNP; Overhauser DNP; Photo-CIDNP; PHIP; SEOP; Fast NMR

1. Basic concepts and well-established advances

Fundamental concepts

While early nuclear magnetic resonance observations were performed on bulk materials and simple molecules such as paraffin and water [1], the technique has now become much more sophisticated and NMR data are routinely collected in solution on dilute biological macromolecules at concentrations typically ranging from 100 μM to 10 mM. The atomic resolution of NMR spectroscopy and its high information content, which includes both structure and dynamics in solution [2], render it an exceptional tool in biology. Yet the poor sensitivity of NMR is still a challenge.

For spin-1/2 nuclei, the magnetization, which is proportional to the NMR resonance intensity (i.e., the signal), can be generally defined as

*To whom correspondence should be addressed: Silvia Cavagnero, Department of Chemistry, University of Wisconsin-Madison, 1101 University Avenue, Madison, Wisconsin 53706, USA, Phone: 608-262-5430, Fax: 608-262-9918, cavagnero@chem.wisc.edu.

$$M=\frac{\gamma\hbar N}{2}P, \quad (1)$$

where γ denotes the nuclear gyromagnetic ratio, $\hbar$ is the Planck's constant divided by 2π, N is the total number of spins, and P is the nuclear polarization, defined as

$$P=\frac{N_\alpha-N_\beta}{N_\alpha+N_\beta}=\frac{N_\alpha-N_\beta}{N}, \quad (2)$$

where N_α and N_β are the number of α and β spins, respectively. It is useful to keep in mind that P is often expressed as a percent polarization $P_{\%}$, with $P_{\%} = P \times 100$.

At thermal equilibrium, the Boltzmann distribution applies, and the above relations can be expressed as

$$P=\frac{N_\alpha-N_\beta}{N_\alpha+N_\beta}=\frac{\exp\left(\frac{\gamma\hbar B_o}{2k_B T}\right)-\exp\left(-\frac{\gamma\hbar B_o}{2k_B T}\right)}{\exp\left(\frac{\gamma\hbar B_o}{2k_B T}\right)+\exp\left(-\frac{\gamma\hbar B_o}{2k_B T}\right)}=\tanh\left(\frac{\gamma\hbar B_o}{2k_B T}\right), \quad (3)$$

where T is the absolute temperature, B_0 is the applied magnetic field and k_B is the Boltzmann constant [3]. At physiologically relevant temperatures, $P_{\%}$ is extremely small even at very high applied fields. For instance, the ^1H percent polarization in a 1,000 MHz NMR spectrometer is only 0.008% at room temperature.

Despite the small intrinsic polarization, spectroscopic sensitivity can be high if the noise level is small. This concept follows from the definition of sensitivity [4] expressed as signal-to-noise per unit time

$$\left(\frac{S}{N}\right)_t=\frac{S}{2\sigma_N\sqrt{t}}\cong\frac{2.5\times S}{\langle N_{ptp}\rangle\sqrt{t}}. \quad (4)$$

In the above relation, S is the signal peak amplitude, t is the total NMR experimental time, σ_N is the r.m.s. noise amplitude, and $<N_{ptp}>$ is the peak-to-peak noise amplitude within 100 zero crossings, where $<N_{ptp}> \approxeq 5.0\ \sigma_N$ [4]. Here, the term amplitude is regarded as equivalent to height. Note that both S and σ_N are known to be intrinsically time-dependent and to increase linearly with t and $\sqrt{t}$, respectively [4]. Therefore, dividing the signal-to-noise ratio by $\sqrt{t}$ in eq. (4) renders the NMR sensitivity $(S/N)_t$ independent of the total experiment time.

A more explicit description of the magnetic field (B_o) and gyromagnetic ratio (γ) dependence of the signal-to-noise S/N can be obtained upon considering: 1) the relation $M \propto \gamma^2 B_o$, which is evident from eqns (1) and (3) when $\frac{\gamma\hbar B_o}{2k_B T} \ll 1$, 2) the linear dependence of the voltage measured across the NMR receiver coil on γB_o, i.e., the magnetization oscillation frequency, and 3) the noise dependence on $(\gamma B_o)^{1/2}$. The combination of the above effects yields [5–7]

$$\left(\frac{S}{N}\right) \sim \frac{(\gamma^2 B_o)\ (\gamma B_o)}{(\gamma B_o)^{1/2}} \sim {B_o}^{3/2} \gamma^{5/2}. \quad (5)$$

Note that, depending on different assumptions on noise level and instrumental factors, slightly different B_o and γ power dependencies of S/N have in some cases been reported [8, 9].

Remarkably, a number of key advances in NMR over the last few decades led to remarkable improvements in sensitivity. As a result, the current sensitivity of NMR spectroscopy is not so different from that of other techniques characterized by much more favorable Boltzmann factors (e.g., electron paramagnetic resonance, infrared spectroscopy). However, NMR sensitivity is currently largely inferior to that of other spectroscopic techniques, e.g., fluorescence, whose detection limit has recently been stretched down to the single-molecule level. This review documents ongoing efforts to render solution NMR a more sensitive technique, with emphasis on biomolecular applications.

Some well-established advances

Given that the NMR signal-to-noise increases nonlinearly with magnetic field B_o (i.e., proportional to ~ ${B_o}^{3/2}$, see eqn (5)), high applied magnetic fields have been traditionally recognized as the most straightforward means to enhance NMR sensitivity. The introduction of superconducting magnets paved the way to enhanced spin polarization at very high fields, nowadays reaching up to 23.5 T (corresponding to 1,000 MHz). In addition, Fourier-transform pulsed NMR, delivering short radiofrequency pulses covering a wide range of excitation frequencies at once, eliminated the need for frequency scanning and enabled the fast accumulation of multiple transients in a short time, leading to a dramatic ≥ 100-fold increase in sensitivity [4]. Receiver coils composed of materials with very small magnetic susceptibility enabled minimal magnetic field distortions, improving lineshapes and signal-to-noise. The active sample volume has also increased due to improvements in shimming technology, leading to a larger number of detectable NMR-active nuclei [10]. The use of analog filters in combination with time-domain oversampling followed by digital filtering led to the elimination of aliased noise, contributing to improved sensitivity [3, 10]. Recently, the introduction of cryogenic probes led to a significant reduction in noise level via cooling of receiver coils and preamplifiers down to approximately 20 K and 80 K, respectively [11].

Heteronuclear NOE (Nuclear Overhauser Effect) [12] can be employed when sensitive and insensitive nuclei are in close spatial proximity. For instance, ^{1}H saturation, producing steady-state NOE, leads to higher ^{13}C sensitivity. In addition, INEPT (Insensitive Nuclei Enhanced by Polarization Transfer) [13] pulse scheme can be used to transfer magnetization from sensitive to insensitive nuclei in the presence of scalar coupling between the two. In many heteronuclear pulse sequences, INEPT is followed by reverse INEPT (transfer of magnetization back to the sensitive nuclei for detection). Here, the Preservation of Equivalent Pathways (PEP) method [14] can be used to gain sensitivity improvements by factors up to $\sqrt{2}$ relative to the typical reverse INEPT.

Various isotopic labeling strategies were recently developed to maximize NMR sensitivity and resolution in large biomolecules or complex mixtures [15, 16]. ^{13}C- and ^{15}N-enriched biomolecules are no longer limited by natural abundance, and ^{2}H-enrichment leads to reduced dipolar cross-relaxation and spin diffusion [17]. NMR pulse sequences tailored to these isotope labeling schemes have rendered them maximally useful [2, 18]. In addition, NMR tubes matching the susceptibility of the glass to that of water (e.g., Shigemi tubes) and

specialized microcoil/small-volume sample-tube setups help maximizing NMR sensitivity in experiments limited by small amounts of material [19, 20].

2. Methods taking advantage of relaxation rates and chemical shift evolution

Sensitivity enhancement via fast pulsing techniques

Reduction of data collection time to achieve a given S/N is a powerful strategy to enhance NMR sensitivity. Pulse sequences belonging to the SOFAST HMQC class [21, 22] enable fast pulsing by combining multiple strategies to shorten experiment time without significant losses in S/N. First, selective excitation of amide protons leads to fast $^{1}H^{N}$ T_1 relaxation since auto-relaxation is not efficiently compensated by cross-relaxation for slow-tumbling biomolecules in the $\omega_o\tau_c \gg 1$ regime [23, 24], where ω_o is the Larmor frequency and τ_c is the rotational correlation time. Second, Ernst-angle excitation is employed to maximize signal-to-noise per unit time [4]. Both of the above strategies enable dramatic reductions in recycle delay duration. Lastly, the HMQC pulse sequence [25] is employed to minimize the number of selective pulses.

Sensitivity enhancement by attenuation of T_2 relaxation

As seen in eqn. (4), the NMR sensitivity $(S/N)_t$ is directly proportional to signal peak height. Thus, efforts to sharpen NMR resonances by decreasing linewidths (and consequently increasing peak heights) can be regarded as NMR sensitivity enhancement tools. This topic becomes particularly pressing in the case of large biomolecules, characterized by extensive resonance linebroadening.

Linebroadening resulting from large molecular size can be mitigated by Transverse Relaxation Optimized SpectroscopY (TROSY). This method increases the effective spin-spin relaxation time T_2 by selecting the longest-lived coherences resulting from the mutual cancellation of chemical shift anisotropy (CSA) and dipolar relaxation effects [26] or between ^{1}H–^{1}H and ^{1}H–^{13}C dipolar relaxation mechanisms [27]. For instance, when sequential backbone assignments were carried out on the octameric 110 kDa protein 7,8-dihydroneopterin aldolase with both conventional HNCA and [^{15}N,^{1}H]-TROSY-HNCA, a 20- to 50-fold higher sensitivity was achieved with the TROSY-type experiment [28].

In case linebroadening is caused by conformational exchange, “chemical shift scaling” [29] can be used to shift the exchange regime from intermediate to fast on the NMR chemical shift timescale, leading to sharper linewidths [30, 31]. This concept can be implemented by applying the CPMG [32] or WAHUHA [33] based four-pulse trains during the chemical shift evolution time.

The methods described so far start from a Boltzmann distribution of nuclear spin states. In contrast, methods able to shift the thermal nuclear spin populations, illustrated in Figure 1 and compared in Table 1, provide an alternative avenue to enhance NMR sensitivity. It is important to note that strategies to increase NMR sensitivity usually add up in a cumulative fashion, leading to the current state-of-the-art. This idea suggests that further advances, including those outlined in the following sections, will not replace but rather improve the current status quo.

3. Dissolution dynamic nuclear polarization

Basic concepts

A recently developed approach known as dissolution DNP creatively exploits dynamic nuclear polarization (DNP), a well-known phenomenon leading to hyperpolarized NMR-active nuclei in the solid state. Given that dissolution DNP involves NMR analysis of liquids, this technique is suitable to study water-soluble biologically relevant samples. This method has become quite popular over the last few years, and dissolution DNP setups are now commercially available (e.g. HyperSense from Oxford Instruments).

In short, a solid, frozen-solution sample at very low temperature (typically 1.1–1.5 K) is polarized in the presence of a radical, e.g. tris {8-carboxyl-2,2,6,6-tetra[2-(1-hydroxyethyl)]-benzo(1,2-d:4,5-d′)bis(1,3)dithiole-4-yl} methyl sodium salt (Trityl OX063) or nitroxide-based 2,2,6,6-tetramethylpiperidine N-oxide (TEMPO) [34] with microwave irradiation. Dynamic nuclear polarization (DNP) [35, 36] transfers polarization from electrons to nuclei upon microwave irradiation at or near the electron Larmor frequency. The sample is then rapidly melted and dissolved in a suitable hot solvent. The dissolved hyperpolarized sample is then rapidly transferred to a conventional liquid-state NMR setup for detection (Fig. 2A) [37, 38].

Ardenkjær-Larsen, Golman and coworkers first examined the polarization of ^{13}C-urea in glycerol with OX063 as a trityl radical (15 mM, at 1.1K, 94 GHz and 100 mW microwave source). They achieved a ^{13}C polarization up to 42% with a build-up time constant τ_{DNP} = 4,900 s in the solid state. Hot water was then rapidly injected into the sample, and the liquid mixture was then transferred within 6 s to a 9.4T NMR magnet for detection. A remarkable fraction of the original ^{13}C polarization was preserved, with a net ^{13}C polarization of 37% observed after dissolution. This amounts to a ^{13}C S/N 44,400-fold larger than that of a reference ^{13}C NMR experiment conducted at 9.4T and at room temperature in the absence of prior hyperpolarization (ignoring the hyperpolarization build-up time) (Fig. 2B and 2C) [37].

In solids, DNP is known to occur via a number of mechanisms known as the solid effect, thermal mixing and the cross effect [36]. The dependence of the observed polarization on microwave frequency led the authors to propose thermal mixing as the operating DNP mechanism, though contributions from Solid Effect could not be ruled out [37, 38].

Relaxation and voyage times

The T_1 relaxation rate of the hyperpolarized nuclei is crucial in dissolution DNP. To preserve the nuclear polarization acquired in the solid state, polarized samples need to be thawed and transferred to the NMR spectrometer faster than the nuclear T_1 relaxation time [37]. Typical dissolution DNP samples experience a ‘voyage time’ as they are transferred from the polarizing magnet to the liquid state NMR magnet. During the voyage time, the sample is exposed to low fields (outside the magnets) of the order of 0.5 mT. T_1 is shorter at low field and even more so in the presence of the paramagnetic polarizing agent. Hence, short and fast voyages as well as removal of the stable free radical are crucial to minimize polarization losses [39].

Addition of the radical scavenger sodium ascorbate during the dissolution step alleviates polarization decays during and after the transfer. This process leads to a ~2-fold extension of the ^{13}C T_1 of acetate (from 40.1 to 72 s) [40]. Attempts to shorten the voyage time included building a special spectrometer consisting of a single dual-isocentre superconducting magnet with 3.35 and 9.4T polarizing and NMR-dedicated regions, respectively, separated by 83

cm. This system allows transferring the polarized sample to the NMR detection region within 2.9 s, i.e., ca. half of the time taken by conventional dissolution DNP systems [41].

In systems with nuclear spin states delocalized over two or more spins, long-lived nuclear spin states can be generated [42–45]. Now, the intramolecular dipole-dipole interaction is symmetric with respect to spin exchange, while the singlet and triplet spin states are antisymmetric and symmetric, respectively. Therefore, the dipole-dipole interaction can't mediate symmetry-breaking singlet-to-triplet transitions [46]. While triplet states are able to relax via intramolecular dipole-dipole interactions within the triplet manifold, singlet nuclear spin states are unable to undergo intramolecular dipole-dipole relaxation and display remarkably long T_1 values, typically ranging between a few tens of seconds and several minutes [46, 47]. Methods relying on this property were able to generated long-lived singlet spin states in the context of dissolution DNP, and thus improve the effectiveness of this approach. For instance, the lifetimes of the Ala-Gly dipeptide H^{α} protons were increased by 7-fold (over the regular T_1) [47], rendering this peptide suitable for dissolution DNP.

Hyperpolarizing agents

In addition to the TEMPO-like or trityl radicals, alternative hyperpolarizing agents like 1,3-bisdiphenylene-2-phenylallyl (BDPA) have recently been proposed [48]. Hyperpolarized [1-^{13}C]pyruvic acid in sulfolane yielded a 14,000 ($P_{\%,13C}$ = 11%) and 12,000 ($P_{\%,13C}$ = 9.7%) sensitivity enhancement (298K, B_o = 9.4T) in the presence of BDPA and trityl OX063, respectively. The polarization build-up time was not taken into account when computing sensitivities. Unlike trityl radicals, BDPA is water-insoluble. Hence it can be conveniently removed from the hyperpolarized solution by filtration during the dissolution step.

Cross-polarization enhancement of low-γ nuclei

High-γ nuclei like ^{1}H polarize fast and efficiently, yet have short T_1, hence they tend to depolarize fast during transfer to the NMR magnet. Jannin *et al.* carried out experiments showing that cross polarization (CP) from ^{1}H to ^{13}C leads to rapid and significant increase in ^{13}C polarization under typical dissolution DNP conditions [49]. Batel *et al.* went further and showed that, after CP in the solid state, ^{13}C polarization is mostly preserved upon dissolution and detection [50]. These researchers employed 4.5M ^{13}C-urea doped with 30mM TEMPO. The sample was first hyperpolarized (build-up time constants: τ_{1H} = 580 s and τ_{13C} = 1014 s) followed by CP, which doubled ^{13}C polarization, ending up with a final solid-state polarization of 14% achieved within half of the regular build-up time. The ^{13}C polarization after dissolution was retained to a significant level (8.8%). Even higher ^{13}C polarization levels ($P_{\%,13C} \approx 45\%$ in the solid state and $P_{\%,13C} \approx 40\%$ in solution at 300K) were achieved by performing CP at the higher polarizing field of 6.7 T [51].

Additional hyperpolarization enhancers

Addition of lanthanide ions like gadolinium (Gd^{3+}) and holmium (Ho^{3+}) was shown to further enhance the ^{13}C polarization of pyruvate in the solid state. Unfortunately, lanthanides also reduce ^{13}C T_1 values in the liquid state, preventing the use of this strategy in dissolution DNP. However, it was recently shown that addition of chelating agents such as diethylenetriamine pentaacetate (DTPA) during the dissolution process drastically reduces the liquid-state relaxivity of Gd^{3+}, thus minimizing liquid-state relaxation [52]. Hence this method is potentially useful for further increases in NMR sensitivity by dissolution DNP.

2D experiments

An unavoidable drawback of dissolution DNP is the inability to perform iterative DNP, freeze-thaw and transfer steps, limiting multidimensional NMR applications.

Yet, a variety of methods to collect 2D NMR data have recently been developed. These include small-tip-angle excitation [53], spatially encoded ultrafast 2D NMR [54], scaling of heteronuclear coupling by optimal tracking (SHOT) [55], hyper single-point amplitude-separated multi-dimensional (SPASM) NMR [56] and hyperpolarized Hadamard spectroscopy [57].

In situ temperature jump DNP

Griffin *et al*. developed an alternative approach to hyperpolarize samples in the liquid state. The sample is frozen at 90K and ^{1}H is polarized with a biradical polarizing agent (5T, 140GHz microwave source). Polarization is then transferred to low-γ spins via cross polarization. The sample is then melted by irradiation with an infrared pulsed laser, followed by NMR detection (with ^{1}H decoupling) within the same device. An advantage of this method is that it enables iterative hyperpolarization cycles, given that sample melting and NMR spectroscopy are performed *in situ*. Therefore, the entire cycle can be repeated and signal averaging can be performed [58].

Additional applications

Extensive dissolution DNP investigations have been carried out to probe the metabolic activity of tissues (e.g. heart, liver, tumor cells) [38]. For instance, hyperpolarized [1-^{13}C]pyruvate is used as a clinical diagnostic tool in metabolic imaging to characterize differences between normal and tumorigenic cells [59]. Additional applications of more biophysical nature include real-time enzyme kinetics [60], studies of biosynthetic pathways [60], detection of poorly-populated reaction intermediates [61], and ligand-detected protein-ligand interactions [62]. Recently, the pH-jump-induced refolding of the hyperpolarized ribosomal protein L23 was studied in real time by monitoring the time course of the ^{13}C NMR signal intensities [63].

4. Overhauser dynamic nuclear polarization

Unlike the dramatic polarization enhancements achieved in solid-state DNP, which are close to the theoretical limit, smaller enhancements are typically observed in liquid-state Overhauser DNP. Here we briefly review the origin of the Overhauser DNP enhancement (Fig. 3A and 3B), recent efforts to increase them, and some representative applications.

Polarization transfer can occur in solution via the well-known Overhauser effect, which was first observed by Albert Overhauser in 1953 [35] and proceeds via dipolar and scalar interactions between an unpaired electrons and a nearby NMR-active nucleus [64]. The Overhauser enhancement factor, which expresses the enhancement of nuclear polarization in the presence of nearby saturated electrons, is expressed as [64]

$$\varepsilon = \frac{\langle I_z \rangle - I_{eq}}{I_{eq}} = \xi f s \frac{\gamma_e}{\gamma_n}, \quad (6)$$

where $\langle I_z \rangle$ is the longitudinal magnetization, I_{eq} is the equilibrium magnetization, ξ is the coupling factor, f is the leakage factor, s is the saturation factor, γ_e is the gyromagnetic ratio of the electron, and γ_n is the gyromagnetic ratio of the nucleus. The coupling factor (ξ) represents the efficiency of electron-nucleus cross-relaxation, the leakage factor (*f*) describes

the portion of nuclear relaxation due to the electron, and the saturation factor (*s*) reflects the efficiency of microwave pumping. The main challenges to the study of biomolecules via Overhauser DNP are discussed below. First, the coupling factor ξ decreases with magnetic field and molecular size in liquids, where the dipolar contribution to ξ dominates over the scalar contribution [64, 65]. Second, high-power microwave irradiation is necessary to achieve high saturation factors, and this often results in sample heating, especially at high polarizing fields. Third, performing the experiment at physiologically relevant temperatures limits the maximum achievable electron and nuclear polarization to a few percent even with modern superconducting magnets as shown in eqn (3) and discussed by Günther [38].

Regardless of the initially prepared nuclear polarization, the NMR S/N increases with B_0, as shown in eqn (5). In addition, spectral resolution increases at high field [3]. Thus, high fields are generally desirable in liquid-state NMR. Therefore, a major challenge of Overhauser DNP as an NMR sensitivity-enhancement tool is the decrease in coupling factor ξ at high applied fields. Specifically, ξ is proportional to B_0^{-2} for rotational-diffusion-mediated relaxation, and to $B_0^{-3/2}$ for translational-diffusion-mediated relaxation. The coupling factor ξ becomes proportional to B_0^{-1} in molecular dynamics (MD) simulations that take into account the complex solute-solvent dynamics at atomic detail over a wide range of timescales [66]. Computational predictions on the field dependence of ξ via MD simulations agree well with experimental results [67], as illustrated in Figure 3C. This figure also shows good agreement between experimental data and theoretical predictions obtained from a force-free model. In both cases, translational and rotational correlation times from experimental NMR relaxation dispersion measurements were employed as input parameters.

To overcome the unfavorable magnetic field dependence, shuttle-DNP spectrometers (Fig. 3A) have recently been developed so that nuclei are first polarized by microwave irradiation upon saturation of the EPR transitions at low magnetic field, followed by sample or probe transfer to high field for detection [67]. Note, however, that since initial nuclear polarization increases with applied magnetic field, larger net nuclear polarization can be observed at high fields despite the relatively small coupling and enhancement factors. The use of pulsed microwave sources for coherent polarization transfer provides another potential avenue to overcome the unfavorable field dependence of DNP polarization [67].

Another concern in Overhauser DNP is sample heating due to microwave irradiation. This issue is particularly relevant when irradiation is performed at high magnetic field, where the limited penetration depth necessarily confines sample volumes to a few nanoliters [67]. The shuttle-DNP approach helps overcoming this challenge since at low polarizing field relatively low-frequency microwaves can be employed, enabling the use of more conventional NMR sample volumes (e.g. 0.3 ml) [67]. In addition, the microwave resonant cavities are designed such that the microwave magnetic field component is maximized while the corresponding electric field component is minimized at the sample location [68]. In this way, electron spin transitions are saturated and sample heating is reduced. Pulsed microwave sources can also be employed to achieve a high saturation factor with minimal sample heating [69]. By applying a train of high-power π microwave pulses, similar enhancements to CW-DNP can be achieved at much lower average power, hence producing less overall heating [67].

In liquids, the Overhauser DNP enhancement decreases in the presence of slow molecular diffusion (i.e., when translational correlation times are larger than ~ ns), posing challenges to the application of liquid-state Overhauser DNP to large molecules of biological interest [64, 65]. For instance, when the diffusion of water is slow, a dramatic decrease in water DNP efficiency is observed [70]. The feasibility of studying ubiquitin or even larger biomolecules has been proposed [67], based on the shuttle-DNP polarization of the fast-

rotating methyl groups, whose importance in NMR macromolecular characterization has been established [27].

Water is one of the most popular Overhauser DNP substrates since it gives high DNP polarization enhancements due to its fast rotational and translational diffusion. The absolute value of the water ^{1}H polarization reaches 0.26% at 260 GHz microwave irradiation in a 9.2 T magnet (in high-field DNP experiments) in the presence of the ^{14}N-TEMPOL nitroxide radical (1 M) at 160°C (Fig. 3D) [71]. This high temperature results from sample heating at high microwave power. On the other hand, 0.04% was obtained for the absolute value of the Overhauser DNP polarization at 45°C [71], in the presence of lower-power microwave irradiation. The high Overhauser DNP enhancement of small molecules, including water, has been exploited in many applications. For instance, polarization-enhanced water has served as MRI contrast agent [72], and water dynamics has been site-specifically probed near proteins (e.g., myoglobin) in different folding states [70] and in the vicinity of lipid membranes [73] and membrane-protein interfaces [74].

5. Photochemically induced dynamic nuclear polarization

In 1967, a surprising case of NMR-detected nuclear polarization induced by a chemical reaction was originally observed in organic polymerizations promoted by free radical initiators [75] and in halogen-metal exchange processes [76]. Soon thereafter it was discovered that nuclear polarization could also be generated upon photo-excitation of a redox-competent dye in the presence of a biomolecule of interest [77]. This phenomenon, known as photochemically induced dynamic nuclear polarization (photo-CIDNP), has mainly been exploited to study processes such as protein folding and biomolecular interactions, which involve variations in the solvent exposure of specific amino acids since the photo-CIDNP mechanism involves the direct interaction between the photo-excited dye and the substrate of interest [78, 79]. Recent developments, however, have begun to explore the photo-CIDNP effect for NMR sensitivity enhancement purposes in liquid solutions containing biological molecules.

A typical photo-CIDNP sample contains a biomolecule of interest in a liquid solution in the presence of a photoexcitable dye, such as flavin mononucleotide (FMN) or 2,2′-dipyridyl. Sample photo-irradiation (e.g. by an argon ion or a frequency-tripled Nd:YAG laser) directly in the NMR spectrometer may be facilitated by routing the light to the NMR sample tube via an optical fiber (Fig. 4A) [80, 81]. Pulse sequences can be designed to control the relative timing of both the UV-VIS irradiation (to generate photo-CIDNP polarization) and the radio-frequency pulses (to perform the NMR experiment). Present implementations of photo-CIDNP enhance the polarization of nuclei belonging primarily to the Trp, His and Tyr amino acids and all nucleotide bases [79]. Other molecules can potentially be photo-CIDNP-active as long as they (a) are capable of being transiently oxidized by the photoexcited dye and (b) give rise to a radical cation whose EPR g factor bears an appropriate difference with the g factor of the transiently reduced radical anion dye [79].

According to the radical pair mechanism of photo-CIDNP [82, 83], the dye is photoexcited to generate a long-lived (μs – ms) triplet state. Upon encounter of the triplet excited dye with the molecule of interest, one electron (or H$^{\bullet}$) is transiently transferred from the target molecule to the dye, giving rise to a triplet radical pair (Fig. 4B). This radical pair then undergoes either one of two pathways, depending on the nuclear spin state of the molecule of interest.

In the first-case scenario, i.e., when the molecule of interest is in its α nuclear spin state, the radical pair may undergo fast triplet-to-singlet intersystem crossing (TS-ISC). Then, TS-ISC followed by recombination via back-electron transfer produces the original target molecule

with spin preservation in the α state (Fig. 4B). We denote this process as the recombination route. Note that only a singlet radical pair is allowed to undergo recombination. Alternatively, i.e., when the molecule of interest is in its β nuclear spin state, the radical pair may undergo a slower TS-ISC. Then the ion pair is more likely to dissociate before undergoing TS-ISC, and the target molecule would undergo paramagnetic nuclear relaxation to produce comparable populations of α and β spins (Fig. 4B). We denote this process as the escape route. Note that the specific route followed by the α and β spins switches, when the sign of either the hyperfine coupling constant A or Δg changes (see eqn (10)). Importantly, the actual difference between the TS-ISC rates of the α and β spins determines the relative flux through the recombination and escape routes and is, in turn, proportional to the extent of photo-CIDNP.

At a more quantitative level, the TS ISC rate (ω_{TS}) can be expressed as [79, 84]

$$\omega_{TS} = |\omega_M - \omega_D|, \quad (7)$$

where ω_M and ω_D are the unpaired electron EPR precession frequencies of the radical cation state of the target molecule $M^{+\bullet}$ and the radical anion state of the dye $D^{-\bullet}$, respectively. In the simple case of a target molecule carrying only one NMR-active spin ½ nucleus, we have

$$\omega_M = g_M \mu_B B_o/\hbar \pm A/2 \quad \text{and} \quad \omega_D = g_D \mu_B B_o/\hbar, \quad (8)$$

where g_M and g_D are the g-factors of $M^{+\bullet}$ and $D^{-\bullet}$, respectively, μ_B is the Bohr magneton, B_o is the applied magnetic field, and A is the hyperfine coupling constant between the unpaired electron and the unique NMR-active nucleus in $M^{+\bullet}$. The + and − signs apply to the α and β nuclear spin states, respectively. It follows from eqns. (7) and (8) that, for radical pairs containing a spin ½ nucleus, the TS-ISC rate is

$$\omega_{TS} = \Delta g \, \mu_B B_o/\hbar \pm A/2, \quad (9)$$

where Δg is the difference between the g factors of $M^{+\bullet}$ and $D^{-\bullet}$. The TS-ISC probability for the α and β spins is given by

$$\begin{aligned} P_{TS,\alpha} &= \sin^2 \frac{\omega_{TS,\alpha}}{2} t = \sin^2 \left(\frac{\Delta g \, \mu_B B_o}{2\hbar} + \frac{A}{4} \right) t \\ P_{TS,\beta} &= \sin^2 \frac{\omega_{TS,\beta}}{2} t = \sin^2 \left(\frac{\Delta g \, \mu_B B_o}{2\hbar} - \frac{A}{4} \right) t \end{aligned} \quad . \quad (10)$$

The photo-CIDNP signal intensity increases with $|P_{TS,\alpha} - P_{TS,\beta}|$. Hence, as evident from the above relation, the efficiency of photo-CIDNP depends critically on the hyperfine coupling constant A, the applied field, and the Δg value, in addition to other factors including the redox properties of the dye, the molecule of interest and the accessibility of the molecule of interest to physical collision with the dye.

The effect of magnetic field strength on photo-CIDNP is highlighted by the following experiments [85–87]. The applied magnetic field was varied between 0 and 7 Tesla to monitor His, Tyr and Trp photo-CIDNP in the presence of the 2,2′-dipyridyl dye. For Tyr, His and Trp the maximum net photo-CIDNP (longitudinal one-spin order) was observed at ca. 2, 7 and >7 Tesla, respectively. The origin of the observed variation in maximum photo-CIDNP response is likely due to the g-factor difference between amino acid and dye.

As previously mentioned, photo-CIDNP has recently been developed into a promising NMR sensitivity enhancement tool. ^{1}H CIDNP and ^{1}H CIDNP followed by ^{1}H-^{15}N HSQC (*light*) on Trp indole NH were shown to provide ~ 6.5-fold higher enhancement than corresponding *dark* experiments acquired in the absence of laser irradiation [88]. This result corresponds to a ~ 0.03% ^{1}H polarization, assuming that resonance intensity is proportional to polarization. Photo-CIDNP-enhanced versions of the ^{1}H-^{15}N HMQC and SOFAST-HMQC pulse sequences were also developed [89].

As originally shown by Hore and coworkers [88], ^{15}N photo-CIDNP followed by ^{1}H detection provides another convenient route to enhance NMR sensitivity. This approach exploits the high hyperfine coupling between the Trp unpaired electron and the indole nitrogen together with the sensitivity of ^{1}H NMR to provide 100-fold higher sensitivity than a reference dark experiment. While this effect corresponds to only a moderate ~ 0.05% ^{15}N polarization, it leads to a ~ 10-fold higher sensitivity than a reference pulse-field-gradient sensitivity-enhanced ^{1}H-^{15}N HSQC experiment. In addition, advanced pulse schemes exploiting both ^{1}H and ^{15}N photo-CIDNP in the context of ^{1}H-detected heteronuclear correlation have also been developed [90].

The high ^{13}C hyperfine coupling constants and the presence of several CH bonds in aromatic amino acids led to the development of ^{1}H-detected ^{13}C CIDNP in the context of heteronuclear correlation spectroscopy [91]. Up to 16-fold higher sensitivity than a reference sensitivity-enhanced HSQC was achieved, corresponding to ~ 0.08% ^{13}C polarization. Several CH bonds of Trp, Tyr and Trp were enhanced in this experiment, including $^{\alpha}$CH bonds.

In addition to the high photo-CIDNP effect of the ^{13}C and ^{15}N heteronuclei, engineering amino acids containing other heteronuclei with potentially high hyperfine coupling constants provides another route to enhance photo-CIDNP sensitivity. For instance, up to 40-fold sensitivity enhancement (~ 0.18% polarization) was observed for the ^{19}F nucleus (in the 3-fluorotyrosine - FMN pair), which has a high gyromagnetic ratio and a high hyperfine coupling constant upon transient 3-fluorotyrosine oxidation [92].

One major advantage of photo-CIDNP is that it can be performed under mild solution conditions, given that no freeze-thaw cycles or extrinsic stable radicals are required. This feature enables multiple transients to be collected within short time spans, providing the opportunity to increase S/N by signal averaging and/or acquire multidimensional photo-CIDNP data. In practice, however, dye photoreduction (typically FMN to $FMNH_2$) and sample photodegradation mediated by singlet oxygen impose severe limitations on sample integrity and prevent prolonged photo-CIDNP data collection.

In order to promote the necessary reoxidation of $FMNH_2$ to FMN, two strategies have been employed. First, mechanical mixing of the NMR sample between scans served to facilitate oxidation of $FMNH_2$ by ambient oxygen [93]. Alternatively, hydrogen peroxide was added to the sample as an $FMNH_2$ oxidant [93]. In addition, the effect oxygen level on photo-CIDNP was monitored [94]. Saturation of ambient oxygen to facilitate $FMNH_2$ reoxidation caused quenching of triplet-excited dyes, eliminating photo-CIDNP. Likewise, depletion of ambient oxygen to prevent O_2-dependent sample photodegradation caused inefficient reoxidation of $FMNH_2$. More recently, simultaneous prevention of sample photodegradation and dye photoreduction has been achieved by the development of a tailored additive known as the NR-GO-CAT tri-enzyme system [95]. This trio of commercially available enzymes, added to NMR samples in minute catalytic amounts, prevents oxygen-mediated sample degradation and facilitates the efficient and specific reoxidation of $FMNH_2$ in photo-CIDNP experiments. This strategy enabled prolonged photo-CIDNP on amino acids, the σ^{32} peptide

and the drkN SH3 protein at micromolar concentrations, and led to 48-fold greater NMR sensitivity than the reference HSQC experiment.

The latter experiment leads to ~ 0.23% ^{13}C polarization, corresponding to a ~190-fold ^{13}C polarization enhancement relative to the Boltzmann distribution. This result paves the way to long-term photo-CIDNP data collection, which was impossible before. Thanks to the tri-enzyme system, the photo-CIDNP polarization enhancement is achieved iteratively within an experiment, and complex biomolecules can be analyzed in solution at low micromolar concentrations.

Photo-CIDNP experiments at low magnetic field directly (de)populate singlet nuclear spin states of His β H's with long-lived (ca. 1 min) longitudinal magnetization, suggesting promising *in vivo* applications [96].

A pulse sequence for iteratively accumulating photo-CIDNP within a spin system before readout was developed [97]. This strategy is helpful when periodic pulsed laser light sources are employed. Finally, a remarkable ~ 4% ^{13}C polarization, corresponding to a ~10,000-fold ^{13}C NMR sensitivity enhancement, was recently achieved via photo-CIDNP for a bacterial photosynthetic reaction center [98]. The high polarization, which is currently the highest achieved via photo-CIDNP in liquids and is specific to this system, stems from the persistence of large anisotropic components in the hyperfine coupling, within the electron-donor chlorophyll radical. Three photo-CIDNP mechanisms, denoted as three-spin mixing, differential decay and differential relaxation were shown to prevail when the electron donor and acceptor members of the radical pair tumble very slowly and are at a nearly invariant relative distance and orientation [99, 100].

6. Parahydrogen-induced polarization

Molecular hydrogen comes in two isomers, ortho and para, which have symmetric (triplet) and antisymmetric (singlet) nuclear spin states, respectively. The ortho and para isomers are populated as a 3:1 ratio at room temperature, with the ortho isomer being more populated [101]. Interconversion between the two isomers is symmetry forbidden and occurs very slowly. Thus, when hydrogen is flowed through an appropriate paramagnetic catalyst, especially at low temperature (~ 20 K) where parahydrogen is much more stable than orthohydrogen, close to 100% parahydrogen population can be achieved and exploited at ambient temperature [102]. In para-hydrogen-induced polarization (PHIP), nuclear polarization is attained by transferring the high spin order of parahydrogen to the molecule of interest [101] (Fig. 5A).

Typically, PHIP applications involve the direct incorporation of parahydrogen into unsaturated organic molecules via hydrogenation. The new chemical environment experienced by the two protons upon hydrogenation breaks the singlet symmetry and renders the spin system detectable by NMR. Depending on whether hydrogenation is carried out at high or low magnetic field (followed by sample transfer and detection at high magnetic field), the PHIP methods are known as PASADENA [103] or ALTADENA [104], respectively (Fig. 5A). In PASADENA (Parahydrogen and Synthesis Allow Dramatically Enhanced Nuclear Alignment), the parahydrogen singlet symmetry is immediately broken upon hydrogenation due to the distinct chemical shift environment of the two incorporated protons at high magnetic field, and the singlet $\frac{1}{\sqrt{2}}(|\alpha\beta\rangle - |\beta\alpha\rangle)$ parahydrogen is collapsed into two eigenstates, $|\alpha\beta\rangle$ and $|\beta\alpha\rangle$. Thus the NMR spectrum shows two antiphase multiplets. In ALTADENA (Adiabatic Longitudinal Transport after Dissociation Engenders Net Alignment), since the chemical shifts are essentially the same when parahydrogen is incorporated into the substrate at low magnetic field, the singlet state becomes selectively

polarized as $|\alpha\beta\rangle$ or $|\beta\alpha\rangle$ upon adiabatic transfer to high magnetic field. In this case the NMR spectrum is characterized by two hyperpolarized resonances of opposite sign. In case there are other nuclei in the substrate, NOE, scalar and dipolar coupling can cause spin order to spread throughout the substrate during the initial low-field step [101]. Nuclear polarizations of ~ 100% were observed [105] and 0.1 μM concentrations of pyridine [106] were monitored via inorganic-complex-based PHIP.

Despite the high polarization achieved by PHIP, the method is not generally applicable to biomolecules due to the necessary covalent sample modifications. Recently, a very interesting related methodology known as Signal Amplification by Reversible Exchange (SABRE, or Non-Hydrogenative Parahydrogen-Induced Polarization; NH-PHIP; Fig. 5) [107] was developed to polarize substrates in the absence of hydrogenation. In the SABRE experiment, substrate and parahydrogen establish transient contacts via a metal center. While the complex is formed, nuclear polarization is transferred from the ^{1}H nuclei derived from parahydrogen to the molecule of interest. After the polarization transfer, the highly polarized intact substrate is released. Pyridine has been the most popular substrate for SABRE and up to ~11.5 % ^{1}H polarization has been achieved [108]. Remarkably, SABRE shows promise to extend its substrate to other small molecules including short polypeptides [109].

The SABRE approach is similar to ALTADENA in that polarization by parahydrogen occurs at low magnetic field. Interestingly, the magnetic field dependence of the SABRE signal changes very little with substrate type or proton position [110]. This result is in line with the theoretical prediction that the extent of polarization depends primarily on the scalar coupling between two parahydrogen-derived protons but not on the scalar coupling between parahydrogen-derived and substrate protons, within the metal complex [111]. Unlike ALTADENA, however, SABRE does not necessarily involve adiabatic sample transfer to high magnetic field for detection, and optical atomic magnetometer or SQUID devices can be employed for detection even at low magnetic fields [112].

7. Optical pumping

Optical pumping utilizes the ability of circularly polarized light to selectively excite a specific quantum state of an alkali metal, typically Rubidium (Rb). Excellent reviews are available on this topic [113] and we will limit our survey to the basic principles and most exciting applications relevant to the quest for high NMR sensitivity within the biological context. For instance [113], if right (with respect to an external magnetic field) circularly polarized light σ^+ is applied to the $^2S_{1/2}$ ground state of Rb vapor, the Rb atoms carrying a total electron azimuthal angular momentum quantum number $m_J = -1/2$ are selectively excited to the $^2P_{1/2}$ state with $m_J = +1/2$. Note that this discussion neglects the Rb electron-nucleus hyperfine coupling, for simplicity. The above photo-excitation process is usually carried out in a N_2 gas atmosphere to promote nonradiative relaxation and prevent deleterious radiation trapping [113, 114]. Indeed, collision of gaseous N_2 with the excited alkali-metal promotes nonradiative conversion to the $^2S_{1/2}$ ground states that have either $m_J = +1/2$ or $m_J = -1/2$. Because the right polarized light is unable to excite $^2S_{1/2}$ Rb with $m_J = +1/2$, this state will not get depopulated. As a result of continuous light absorption and subsequent relaxation, including spontaneous emission and collision-induced nonradiative relaxation, a large number of atoms accumulate in the $^2S_{1/2}$ state with $m_J = +1/2$ (Fig. 6A).

After the above electron polarization step, spin-exchange between the polarized Rb and a noble gas takes place (Fig. 6B). This process is mediated by the hyperfine interaction, which enables the transfer of electron spin polarization of Rb to the nuclear spin of the noble gas [113]. As a result, enhanced nuclear spin polarization is observed for the noble gas.

Polarizations greater than 50% (Fig. 6C and 6D) and about 80% have been reported for ^{129}Xe [115, 116] and ^{3}He, respectively [117]. The polarization build-up time depends on experimental conditions. For instance, 7.5% of the xenon polarization is achieved in 5 min at 2.2 atm pressure [118].

^{3}He and ^{129}Xe are the most commonly used noble gases for spin-exchange optical pumping (SEOP). ^{129}Xe, whose natural abundance is 26%, is particularly useful in the context of biology because, in addition to its chemical inertness, it is highly polarizable due to its large electron cloud. Hence ^{129}Xe NMR is extremely sensitive to the surrounding environment and can be used at low concentrations, despite the moderately small value of this nucleus' gyromagnetic ratio (ca. 3.8 times smaller than ^{1}H) [119, 120]. For instance, xenon dissolves in water up to 190 μM at 310 K and 0.058 atm partial pressure [121]. In addition, ^{129}Xe is one order of magnitude more soluble than ^{3}He in biologically relevant fluids such as water and blood at room temperature [122].

Among the numerous ^{129}Xe applications reported so far [123, 124], those based on the spin-induced nuclear Overhauser effect (SPINOE) are particularly promising. SPINOE takes advantage of the cross-relaxation between hyperpolarized ^{129}Xe and neighboring ^{1}H spins to accomplish polarization transfer to the protons. Hence, this effect enhances NMR sensitivity for the detection of protons in solution [122, 125]. SPINOE was used primarily to study organic molecules containing xenon-accessible cavities such as α-cyclodextrin and cryptophane-A [123] as well as in the context of proteins larger than 100 amino acids [126]. The hydrophobic cavity of the 10 kDa protein β-cryptogein was studied by SPINOE at 1.6 mM in the presence of 5.2 mM ~15% hyperpolarized xenon. A small but clearly distinguishable increase in ^{1}H resonance intensity (by ~1%) was observed in the inner core of the protein [127]. Additional details about SPINOE can be found elsewhere [122].

Xenon has also been used as a biosensor so that the presence of certain molecules, rather than their conformational features, can be detected at high sensitivity. Xe-based molecular sensors consist of three parts: a cage containing hyperpolarized ^{129}Xe, a ligand head designed to bind the chosen target with high affinity, and a tether linking the above components. Binding of the ligand head to the target molecule is sensed via ^{129}Xe NMR chemical shifts, so that quantitative information on the amount of bound protein ligand can be gained [123, 128]. One of the most commonly used cages is cryptophane-A, and various cryptophane derivatives as well as other potential cages (e.g., cucurbit[6]uril and cucurbit[5]uril derivatives) have also been explored [120, 129].

To further increase NMR sensitivity, ^{129}Xe hyperpolarization and chemical exchange saturation transfer (CEST) were combined in Hyper-CEST [130]. The spin pool of Xe atoms encapsulated in the cage is saturated by frequency-selective radiofrequency pulses and transferred by chemical exchange to the larger free Xe spin pool in solution. This results in a decrease in signal by the free bulk hyperpolarized Xe. This effect is indicative of the presence of caged Xe, hence it reports on the presence of the target molecule.

A ^{129}Xe NMR experiment with direct (5 %) Xe hyperpolarization provides ~10^{4} higher sensitivity than a reference experiment with unpolarized Xe, disregarding the polarization buildup time. Hyper-CEST provides a further ~4000-fold sensitivity enhancement relative to the direct-hyperpolarized Xe experiment [121]. Hence, hyper-CEST achieves an unprecedented overall increase in sensitivity by seven-orders of magnitude relative to the unpolarized Xe experiment, disregarding the Xe hyperpolarization build-up time [120]. Finally, a newly developed ^{129}Xe Hyper-CEST agent based on readily prepared perfluorocarbon (PFC) nanoemulsion droplets shows great promise for easily accessible future applications [131].

8. When sensitivity is not a top priority: rapid data collection schemes

In NMR applications monitoring kinetics in real time and in experiments that require high-dimensionality (≥ 2D), a reduction of the total experiment time can be critically important, even in the case of concentrated samples.

The total data collection time of multidimensional NMR experiments can be significantly shortened by a suite of approaches known as reduced sampling techniques. Hence, in terms of amount of useful data collected per unit time, reduced sampling techniques can be regarded as powerful tools. These approaches include non-uniform sampling (NUS) [132–134] [135], knowledge-based optimized data undersampling [136], and non-Fourier methods like Hadamard spectroscopy [137].

Interestingly, some studies reported that, depending on the sampling strategy and reconstruction method, NUS may give rise to an actual increase in the S/N ratio and “detection sensitivity”, i.e., the probability of detecting weak peaks, compared to uniformly sampled experiments with an identical total data collection time [138]. However, it needs to be noted that NUS often involves reconstruction procedures that require cautious monitoring of the reliability of the output spectral features [139].

In addition, spatially encoded ultrafast nD NMR methods take advantage of parallel data collection in multiple regions of the sample in the presence of fast-switching pulse field gradients. Ultrafast nD NMR enables the acquisition of complete multidimensional NMR spectra within a single scan [140]. This creative technique is capable of yielding rapid spectral output at the cost of a lower sensitivity than the corresponding conventional experiment. On the other hand, the rapid acquisition of multidimensional data renders it ideal for fast kinetic studies on systems that are not concentration-limited [141].

Importantly, the combination of hyperpolarization methods outlined in sections 3–7 with the fast data collection approaches described here is a powerful tool, and has already yielded intriguing results [142]. This strategy bears unique promise for future synergistic improvements in resolution, sensitivity and data collection speed.

9. Additional techniques of potential future relevance

The NMR analysis of liquids is sometimes preceded by a spin hyperpolarization step in the solid or gas phase, as in the dissolution DNP and optical pumping approaches. Thus it is conceivable to anticipate that additional methods, presently employed to hyperpolarize non-liquid samples, may in the future gain additional ground and become amenable to the analysis of more wide-ranging classes of molecules by liquid-state NMR. These methodologies include solid-state photo-CIDNP [99], solid-state DNP [36], the Haupt effect[143], transfer of rotational to nuclear spin polarization [144] and microwave-induced optical nuclear polarization (MIONP) [145].

In addition, nontraditional detection schemes have already succeeded or bear future promise to enhance NMR sensitivity in liquids. In optical magnetometry, for instance, the precession of laser-polarized alkali atoms is probed by laser light to detect small local magnetic fields below femtotesla arising from the NMR samples [146, 147]. Alternatively, superconducting quantum interference devices (SQUID) are able to detect magnetic flux, rather than the rates of magnetic flux change [148]. Both optical magnetometry and SQUID detection are actively used in zero-field and low-field NMR of liquids [112, 149].

In addition, nuclear spin-induced optical rotation (NSOR) has been used to measure variations in the degree of light polarization to detect nuclear spins of liquid water or

liquid ^{129}Xe [150]. Lastly, remote-detection schemes where the spectral information is encoded in one coil and detected in a different coil with optimized filling factor can potentially provide large signal enhancements for ^{129}Xe in liquids [151].

Remarkably, magnetic resonance force microscopy [152] can detect less than 100 nuclear spins of biologically relevant solids by sensing the forces generated by the nuclear magnetic moments of the sample. Finally, the influence of microwave irradiation (which saturates the $T_x \leftrightarrow T_z$ and $T_y \leftrightarrow T_z$ triplet-sublevel transitions) on single-molecule fluorescence enables the indirect detection of the nuclear magnetic moments of the sample at the single-molecule level [153, 154]. The nuclear magnetic moments are coupled to the photoexcited electronic states via the hyperfine interaction, which enables the indirect detection of magnetic resonance by fluorescence.

10. Conclusions

In summary, as shown in the side-by-side comparisons provided in Table 1, the leading techniques capable of improving NMR sensitivity in solution have been able to reach amazing results over the last few years, and have several clear advantages. On the other hand, a lot of work still needs to be done, given the few disadvantages. The shortcomings of the methods pose some limits to their applicability to a wide number of NMR-active nuclei and complex biomolecules as well as, in some cases, to long-term data collection. Despite these undeniable challenges, however, progress is happening fast and we anticipate many further exciting advances in future years.

Acknowledgments

We are grateful to Thad Walker, Charlie Fry, Milo Westler, Marco Tonelli and Zachary Deland for useful discussions. This research was supported by NIH grant R21AI08851 and a UW-Madison Graduate School grant to S.C. In addition, Y.O. is the recipient of an NIH Molecular Biophysics training fellowship.

References

1. Bloch F, Hansen W, Packard M. The nuclear induction experiment. Phys Rev. 1946; 70:474–485.
2. Kay LE. NMR studies of protein structure and dynamics. J Magn Reson. 2005; 173:193–207. [PubMed: 15780912]
3. Cavanagh, J.; Fairbrother, WJ.; Palmer, AG., III; Skelton, NJ. Protein NMR Spectroscopy: Principles and Practice. Academic Press; San Diego: 2007.
4. Ernst, RR.; Bodenhausen, G.; Wokaun, A. Principles of Nuclear Magnetic Resonance in One and Two Dimensions. Oxford University Press; Upper Saddle River: 1989.
5. van de Ven, FJM. Multidimensional NMR in Liquids: Basic Principles and Experimental Methods. Wiley-VCH; New York: 1995.
6. Freeman, R. Handbook of nuclear magnetic resonance. 2. Longman; London: 1997.
7. Abragam, A. The Principle of Nuclear Magnetism. Clarendon Press; Oxford: 1961.
8. Hoult DI, Richards R. The signal-to-noise ratio of the nuclear magnetic resonance experiment. J Magn Reson. 1976; 24:71–85.
9. Harris, RK. Nuclear Magnetic Resonance Spectroscopy: A Physicochemical View. Longman Scientific and Technical; Harlow: 1986.
10. Claridge, TDW. High-Resolution NMR Techniques in Organic Chemistry. 2. Elsevier; Amsterdam: 2009.
11. Kovacs H, Moskau D, Spraul M. Cryogenically cooled probes-a leap in NMR technology. Prog Nucl Magn Reson Spectrosc. 2005; 46:131–155.
12. Solomon I. Relaxation processes in a system of two spins. Phys Rev. 1955; 99:559.
13. Morris GA, Freeman R. Enhancement of nuclear magnetic resonance signals by polarization transfer. J Am Chem Soc. 1979; 101:760–762.

14. Palmer AG, Cavanagh J, Wright PE, Rance M. Sensitivity improvement in proton-detected two-dimensional heteronuclear correlation NMR spectroscopy. J Magn Reson. 1991; 93:151–170.
15. Goto NK, Gardner KH, Mueller GA, Willis RC, Kay LE. A robust and cost-effective method for the production of Val, Leu, Ile (δ1) methyl-protonated 15N-, 13C-, 2H-labeled proteins. J Biomol NMR. 1999; 13:369–374. [PubMed: 10383198]
16. Kainosho M, Torizawa T, Iwashita Y, Terauchi T, Ono AM, Güntert P. Optimal isotope labelling for NMR protein structure determinations. Nature. 2006; 440:52–57. [PubMed: 16511487]
17. Gardner KH, Kay LE. The use of 2H, 13C, 15N multidimensional NMR to study the structure and dynamics of proteins. Annu Rev Biophys Biomol Struct. 1998; 27:357–406. [PubMed: 9646872]
18. Grzesiek S, Anglister J, Ren H, Bax A. 13C line narrowing by 2H decoupling in 2H/13C/15N enriched proteins. Application to triple resonance 4D J connectivity of sequential amides. J Am Chem Soc. 1993; 115:4369–4370.
19. Jones CJ, Larive CK. Could smaller really be better? Current and future trends in high-resolution microcoil NMR spectroscopy. Anal Bioanal Chem. 2012; 402:61–68. [PubMed: 21879299]
20. Webb A. Microcoil nuclear magnetic resonance spectroscopy. J Pharm Biomed Anal. 2005; 38:892–903. [PubMed: 16087050]
21. Schanda P, Brutscher B. Very fast two-dimensional NMR spectroscopy for real-time investigation of dynamic events in proteins on the time scale of seconds. J Am Chem Soc. 2005; 127:8014–8015. [PubMed: 15926816]
22. Gal M, Schanda P, Brutscher B, Frydman L. UltraSOFAST HMQC NMR and the repetitive acquisition of 2D protein spectra at Hz rates. J Am Chem Soc. 2007; 129:1372–1377. [PubMed: 17263421]
23. Pervushin K, Vögeli B, Eletsky A. Longitudinal 1H relaxation optimization in TROSY NMR spectroscopy. J Am Chem Soc. 2002; 124:12898–12902. [PubMed: 12392438]
24. Rossi, C. Selective relaxation techniques in biological NMR. In: Grapt, DM.; Harris, RK., editors. Encyclopedia of NMR. John Wiley & Sons; New York: 1989. p. 4237-4246.
25. Bax A, Griffey RH, Hawkins BL. Correlation of proton and nitrogen-15 chemical shifts by multiple quantum NMR. J Magn Reson. 1983; 55:301–315.
26. Pervushin K, Riek R, Wider G, Wüthrich K. Attenuated T2 relaxation by mutual cancellation of dipole–dipole coupling and chemical shift anisotropy indicates an avenue to NMR structures of very large biological macromolecules in solution. Proc Natl Acad Sci USA. 1997; 94:12366–12371. [PubMed: 9356455]
27. Kay LE. Solution NMR spectroscopy of supra-molecular systems, why bother? A methyl-TROSY view. J Magn Reson. 2011; 210:159–170. [PubMed: 21458338]
28. Salzmann M, Pervushin K, Wider G, Senn H, Wüthrich K. NMR assignment and secondary structure determination of an octameric 110 kDa protein using TROSY in triple resonance experiments. J Am Chem Soc. 2000; 122:7543–7548.
29. Ellett JD, Waugh JS. Chemical shift concertina. J Chem Phys. 1969; 51:2851.
30. Zhuravleva A, Orekhov VY. Divided evolution: a scheme for suppression of line broadening induced by conformational exchange. J Am Chem Soc. 2008; 130:3260–3261. [PubMed: 18293983]
31. Li Y, Palmer AG. Narrowing of protein NMR spectral lines broadened by chemical exchange. J Am Chem Soc. 2010; 132:8856–8857. [PubMed: 20550111]
32. Meiboom S, Gill D. Modified spin-echo method for measuring nuclear relaxation times. Rev Sci Instrum. 1958; 29:688–691.
33. Waugh JS, Huber LM, Haeberlen U. Approach to high-resolution NMR in solids. Phys Rev Lett. 1968; 20:180–182.
34. Lumata LL, Merritt ME, Malloy CR, Sherry AD, van Tol J, Song L, Kovacs Z. Dissolution DNP-NMR spectroscopy using galvinoxyl as a polarizing agent. J Magn Reson. 2012; 227:14–19. [PubMed: 23246650]
35. Overhauser AW. Polarization of nuclei in metals. Phys Rev. 1953; 92:411.

36. Maly T, Debelouchina GT, Bajaj VS, Hu KN, Joo CG, Mak-Jurkauskas ML, Sirigiri JR, van der Wel PCA, Herzfeld J, Temkin RJ, Griffin RG. Dynamic nuclear polarization at high magnetic fields. J Chem Phys. 2008; 128:052211. [PubMed: 18266416]
37. Ardenkjær-Larsen JH, Fridlund B, Gram A, Hansson G, Hansson L, Lerche MH, Servin R, Thaning M, Golman K. Increase in signal-to-noise ratio of > 10,000 times in liquid-state NMR. Proc Natl Acad Sci USA. 2003; 100:10158–10163. [PubMed: 12930897]
38. Gunther UL. Dynamic nuclear hyperpolarization in liquids. Top Curr Chem. 2013; 335:23–69. [PubMed: 22025060]
39. Miéville P, Jannin S, Bodenhausen G. Relaxometry of insensitive nuclei: optimizing dissolution dynamic nuclear polarization. J Magn Reson. 2011; 210:137–140. [PubMed: 21393034]
40. Miéville P, Ahuja P, Sarkar R, Jannin S, Vasos PR, Gerber-Lemaire S, Mishkovsky M, Comment A, Gruetter R, Ouari O, Tordo P, Bodenhausen G. Scavenging free radicals to preserve enhancement and extend relaxation times in NMR using dynamic nuclear polarization. Angew Chem Int Ed. 2010; 122:6318–6321.
41. Leggett J, Hunter R, Granwehr J, Panek R, Perez-Linde AJ, Horsewill AJ, McMaster J, Smith G, Kockenberger W. A dedicated spectrometer for dissolution DNP NMR spectroscopy. Phys Chem Chem Phys. 2010; 12:5883–5892. [PubMed: 20458428]
42. Carravetta M, Johannessen OG, Levitt MH. Beyond the T-1 limit: Singlet nuclear spin states in low magnetic fields. Phys Rev Lett. 2004; 92
43. Carravetta M, Levitt MH. Long-lived nuclear spin states in high-field solution NMR. J Am Chem Soc. 2004; 126:6228–6229. [PubMed: 15149209]
44. Levitt MH. Singlet nuclear magnetic resonance. Annu Rev Phys Chem. 2012; 63:89–105. [PubMed: 22224703]
45. Warren WS, Jenista E, Branca RT, Chen X. Increasing Hyperpolarized Spin Lifetimes Through True Singlet Eigenstates. Science. 2009; 323:1711–1714. [PubMed: 19325112]
46. Carravetta M, Levitt MH. Theory of long-lived nuclear spin states in solution nuclear magnetic resonance. I. Singlet states in low magnetic field. J Chem Phys. 2005; 122:214505. [PubMed: 15974752]
47. Vasos PR, Comment A, Sarkar R, Ahuja P, Jannin S, Ansermet JP, Konter JA, Hautle P, van den Brandt B, Bodenhausen G. Long-lived states to sustain hyperpolarized magnetization. Proc Natl Acad Sci USA. 2009; 106:18469–18473. [PubMed: 19841270]
48. Lumata L, Ratnakar SJ, Jindal A, Merritt M, Comment A, Malloy C, Sherry AD, Kovacs Z. BDPA: An efficient polarizing agent for fast dissolution dynamic nuclear polarization NMR spectroscopy. Chem Eur J. 2011; 17:10825–10827. [PubMed: 21919088]
49. Jannin S, Bornet A, Colombo S, Bodenhausen G. Low-temperature cross polarization in view of enhancing dissolution dynamic nuclear polarization in NMR. Chem Phys Lett. 2011; 517:234–236.
50. Batel M, Krajewski M, Däpp A, Hunkeler A, Meier BH, Kozerke S, Ernst M. Dissolution dynamic nuclear polarization efficiency enhanced by Hartmann–Hahn cross polarization. Chem Phys Lett. 2012; 554:72–76.
51. Bornet A, Melzi R, Perez Linde AJ, Hautle P, van den Brandt B, Jannin S, Bodenhausen G. Boosting dissolution dynamic nuclear polarization by cross polarization. J Phys Chem Lett. 2012; 4:111–114.
52. Gordon JW, Fain SB, Rowland IJ. Effect of lanthanide ions on dynamic nuclear polarization enhancement and liquid-state T1 relaxation. Magn Reson Med. 2012; 68:1949–1954. [PubMed: 22367680]
53. Zeng H, Bowen S, Hilty C. Sequentially acquired two-dimensional NMR spectra from hyperpolarized sample. J Magn Reson. 2009; 199:159–165. [PubMed: 19447055]
54. Mishkovsky M, Frydman L. Progress in hyperpolarized ultrafast 2D NMR spectroscopy. Chem Phys Chem. 2008; 9:2340–2348. [PubMed: 18850607]
55. Zhang G, Schilling F, Glaser SJ, Hilty C. Chemical shift correlations from hyperpolarized NMR using a single SHOT. Anal Chem. 2013; 85:2875–2881. [PubMed: 23350922]
56. Donovan KJ, Frydman L. HyperSPASM NMR: a new approach to single-shot 2D correlations on DNP-enhanced samples. J Magn Reson. 2012; 225:115–119. [PubMed: 23159821]

57. Chen HY, Hilty C. Hyperpolarized Hadamard spectroscopy using flow NMR. Anal Chem. 2013; 85:7385–7390. [PubMed: 23834163]
58. Joo CG, Hu KN, Bryant JA, Griffin RG. In situ temperature jump high-frequency dynamic nuclear polarization experiments: Enhanced sensitivity in liquid-state NMR spectroscopy. J Am Chem Soc. 2006; 128:9428–9432. [PubMed: 16848479]
59. Golman K, Lerche M, Pehrson R, Ardenkjaer-Larsen JH. Metabolic imaging by hyperpolarized 13C magnetic resonance imaging for in vivo tumor diagnosis. Cancer Res. 2006; 66:10855–10860. [PubMed: 17108122]
60. Bowen S, Hilty C. Time-resolved dynamic nuclear polarization enhanced NMR spectroscopy. Angew Chem Int Ed. 2008; 120:5313–5315.
61. Jensen PR, Meier S, Ardenkjær-Larsen JH, Duus JØ, Karlsson M, Lerche MH. Detection of low-populated reaction intermediates with hyperpolarized NMR. Chem Commun. 2009:5168–5170.
62. Lerche MH, Meier S, Jensen PR, Baumann H, Petersen BO, Karlsson M, Duus JØ, Ardenkjær-Larsen JH. Study of molecular interactions with 13C DNP-NMR. J Magn Reson. 2010; 203:52–56. [PubMed: 20022775]
63. Chen HY, Ragavan M, Hilty C. Protein folding studied by dissolution dynamic nuclear polarization. Angew Chem Int Ed. 2013; 52:9192–9195.
64. Hausser K, Stehlik D. Dynamic nuclear polarization in liquids. Adv Magn Reson. 1968; 3:79–139.
65. Hwang LP, Freed JH. Dynamic effects of pair correlation functions on spin relaxation by translational diffusion in liquids. J Chem Phys. 1975; 63:4017.
66. Sezer D, Prandolini MJ, Prisner TF. Dynamic nuclear polarization coupling factors calculated from molecular dynamics simulations of a nitroxide radical in water. Phys Chem Chem Phys. 2009; 11:6626–6637. [PubMed: 19639137]
67. Griesinger C, Bennati M, Vieth H, Luchinat C, Parigi G, Höfer P, Engelke F, Glaser S, Denysenkov V, Prisner T. Dynamic nuclear polarization at high magnetic fields in liquids. Prog Nucl Magn Reson Spectrosc. 2012; 64:4–28. [PubMed: 22578315]
68. Denysenkov V, Prandolini MJ, Gafurov M, Sezer D, Endeward B, Prisner TF. Liquid state DNP using a 260 GHz high power gyrotron. Phys Chem Chem Phys. 2010; 12:5786–5790. [PubMed: 20461255]
69. Korchak S, Kiryutin A, Ivanov K, Yurkovskaya A, Grishin YA, Zimmermann H, Vieth HM. Low-field, time-resolved dynamic nuclear polarization with field cycling and high-resolution NMR detection. Appl Magn Reson. 2010; 37:515–537.
70. Armstrong BD, Choi J, López C, Wesener DA, Hubbell W, Cavagnero S, Han S. Site-specific hydration dynamics in the nonpolar core of a molten globule by dynamic nuclear polarization of water. J Am Chem Soc. 2011; 133:5987–5995. [PubMed: 21443207]
71. Neugebauer P, Krummenacker JG, Denysenkov VP, Parigi G, Luchinat C, Prisner TF. Liquid state DNP of water at 9.2 T: an experimental access to saturation. Phys Chem Chem Phys. 2013; 15:6049–6056. [PubMed: 23493879]
72. McCarney ER, Armstrong BD, Lingwood MD, Han S. Hyperpolarized water as an authentic magnetic resonance imaging contrast agent. Proc Natl Acad Sci USA. 2007; 104:1754–1759. [PubMed: 17264210]
73. McCarney ER, Armstrong BD, Kausik R, Han S. Dynamic nuclear polarization enhanced nuclear magnetic resonance and electron spin resonance studies of hydration and local water dynamics in micelle and vesicle assemblies. Langmuir. 2008; 24:10062–10072. [PubMed: 18700788]
74. Cheng CY, Varkey J, Ambroso MR, Langen R, Han S. Hydration dynamics as an intrinsic ruler for refining protein structure at lipid membrane interfaces. Proc Natl Acad Sci USA. 2013; 110:16838–16843. [PubMed: 24082088]
75. Bargon J, Fischer H, Johnson U. Nuclear magnetic resonance emission lines during fast radical reactions. I. Recording methods and examples. Z Naturforsch A. 1967; 22:1551–1555.
76. Ward HR, Lawler RG. Nuclear magnetic resonance emission and enhanced absorption in rapid organometallic reactions. J Am Chem Soc. 1967; 89:5518–5519.
77. Cocivera M. Optically induced overhauser effect in solution. Nuclear magnetic resonance emission. J Am Chem Soc. 1968; 90:3261–3263.

78. Kaptein R, Dijkstra K, Nicolay K. Laser photo-CIDNP as a surface probe for proteins in solution. Nature. 1978; 274:293–294. [PubMed: 683312]
79. Hore PJ, Broadhurst RW. Photo-CIDNP of biopolymers. Prog Nucl Magn Reson Spectrosc. 1993; 25:345–402.
80. Kuhn LT. Photo-CIDNP NMR spectroscopy of amino acids and proteins. Top Curr Chem. 2013; 338:229–300. [PubMed: 23670104]
81. Goez, M. Photo-CIDNP Spectroscopy. In: Webb, GA., editor. Annual Reports on NMR Spectroscopy. Academic Press; London: 2009. p. 77-147.
82. Kaptein R, Oosterhoff JL. Chemically induced dynamic nuclear polarization II - (relation with anomalous ESR Spectra). Chem Phys Lett. 1969; 4:195–197.
83. Closs GL, Closs LE. Induced dynamic nuclear spin polarization in photoreductions of benzophenone by toluene and ethylbenzene. J Am Chem Soc. 1969; 91:4549–4550.
84. Muus, LT.; Atkins, PW.; McLauchlan, KA.; Pedersen, JB., editors. Chemically Induced Magnetic Polarization. Reidel; Dordrecht: 1977.
85. Fabian H, Grosse S, Onnen M, Vieth HM, Yurkovskaya A. Chemically induced dynamic nuclear polarization (CIDNP) in the photoreaction of N-acetyl histidine, tyrosine, and tryptophan with 2, 2′-dipyridyl and its dependence on the magnetic field. RIKEN Rev. 2002; 44:134–136.
86. Grosse S, Yurkovskaya AV, Lopez J, Vieth HM. Field dependence of chemically induced dynamic nuclear polarization (CIDNP) in the photoreaction of N-acetyl histidine with 2, 2′-dipyridyl in aqueous solution. J Chem Phys A. 2001; 105:6311–6319.
87. Ivanov KL, Vieth HM, Miesel K, Yurkovskaya AV, Sagdeev RZ. Investigation of the magnetic field dependence of CIDNP in multi-nuclear radical pairs. Part II. Photoreaction of tyrosine and comparison of model calculation with experimental data. Phys Chem Chem Phys. 2003; 5:3470–3480.
88. Lyon CE, Jones JA, Redfield C, Dobson CM, Hore PJ. Two-dimensional 15N-1H photo-CIDNP as a surface probe of native and partially structured proteins. J Am Chem Soc. 1999; 121:6505–6506.
89. Sekhar A, Cavagnero S. 1H photo-CIDNP enhancements in heteronuclear correlation NMR spectroscopy. J Phys Chem B. 2009; 113:8310–8318. [PubMed: 19462951]
90. Sekhar A, Cavagnero S. EPIC- and CHANCE-HSQC: Two 15N photo-CIDNP-enhanced pulse sequences for the sensitive detection of solvent-exposed tryptophan. J Magn Reson. 2009; 200:207–213. [PubMed: 19643649]
91. Lee JH, Sekhar A, Cavagnero S. 1H-detected 13C photo-CIDNP as a sensitivity enhancement tool in solution NMR. J Am Chem Soc. 2011; 133:8062–8065. [PubMed: 21548581]
92. Kuprov I, Hore PJ. Chemically amplified 19F-1H nuclear Overhauser effects. J Magn Reson. 2004; 168:1–7. [PubMed: 15082243]
93. Maeda K, Lyon CE, Lopez JJ, Cemazar M, Dobson CM, Hore P. Improved photo-CIDNP methods for studying protein structure and folding. J Biomol NMR. 2000; 16:235–244. [PubMed: 10805130]
94. Connolly PJ, Hoch JC. Photochemical degradation of tryptophan residues during CIDNP experiments. J Magn Reson. 1991; 95:165–173.
95. Lee JH, Cavagnero S. A novel tri-enzyme system in combination with laser-driven NMR enables efficient nuclear polarization of biomolecules in solution. J Phys Chem B. 2013; 117:6069–6081. [PubMed: 23560683]
96. Kiryutin AS, Korchak SE, Ivanov KL, Yurkovskaya AV, Vieth HM. Creating long-lived spin states at variable magnetic field by means of photochemically induced dynamic nuclear polarization. J Phys Chem Lett. 2012; 3:1814–1819.
97. Goez M, Kuprov I, Hun Mok K, Hore P. Novel pulse sequences for time-resolved photo-CIDNP. Mol Phys. 2006; 104:1675–1686.
98. Daviso E, Janssen GJ, Alia A, Jeschke G, Matysik J, Tessari M. A 10,000-fold nuclear hyperpolarization of a membrane protein in the liquid phase via solid-state mechanism. J Am Chem Soc. 2011; 133:16754–16757. [PubMed: 21962225]
99. Thamarath SS, Heberle J, Hore PJ, Kottke T, Matysik Jr. Solid-state photo-CIDNP effect observed in phototropin LOV1-C57S by 13C magic-angle spinning NMR spectroscopy. J Am Chem Soc. 2010; 132:15542–15543. [PubMed: 20958069]

100. Jeschke G, Matysik J. A reassessment of the origin of photochemically induced dynamic nuclear polarization effects in solids. Chem Phys. 2003; 294:239–255.
101. Natterer J, Bargon J. Parahydrogen induced polarization. Prog Nucl Magn Reson Spectrosc. 1997; 31:293–315.
102. Duckett SB, Sleigh CJ. Applications of the parahydrogen phenomenon: a chemical perspective. Prog Nucl Magn Reson Spectrosc. 1999; 34:71–92.
103. Bowers CR, Weitekamp D. Parahydrogen and synthesis allow dramatically enhanced nuclear alignment. J Am Chem Soc. 1987; 109:5541–5542.
104. Pravica MG, Weitekamp DP. Net NMR alignment by adiabatic transport of parahydrogen addition products to high magnetic field. Chem Phys Lett. 1988; 145:255–258.
105. Blazina D, Duckett S, Halstead T, Kozak C, Taylor R, Anwar M, Jones J, Carteret H. Generation and interrogation of a pure nuclear spin state by parahydrogen-enhanced NMR spectroscopy: a defined initial state for quantum computation. Magn Reson Chem. 2005; 43:200–208. [PubMed: 15625721]
106. Wood NJ, Brannigan JA, Duckett SB, Heath SL, Wagstaff J. Detection of picomole amounts of biological substrates by para-hydrogen-enhanced NMR methods in conjunction with a suitable receptor complex. J Am Chem Soc. 2007; 129:11012–11013. [PubMed: 17711281]
107. Adams RW, Aguilar JA, Atkinson KD, Cowley MJ, Elliott PI, Duckett SB, Green GG, Khazal IG, López-Serrano J, Williamson DC. Reversible interactions with para-hydrogen enhance NMR sensitivity by polarization transfer. Science. 2009; 323:1708–1711. [PubMed: 19325111]
108. Cowley MJ, Adams RW, Atkinson KD, Cockett MC, Duckett SB, Green GG, Lohman JA, Kerssebaum R, Kilgour D, Mewis RE. Iridium N-heterocyclic carbene complexes as efficient catalysts for magnetization transfer from para-hydrogen. J Am Chem Soc. 2011; 133:6134–6137. [PubMed: 21469642]
109. Glöggler S, Müller R, Colell J, Emondts M, Dabrowski M, Blümich B, Appelt S. Para-hydrogen induced polarization of amino acids, peptides and deuterium–hydrogen gas. Phys Chem Chem Phys. 2011; 13:13759–13764. [PubMed: 21720644]
110. Dücker EB, Kuhn LT, Münnemann K, Griesinger C. Similarity of SABRE field dependence in chemically different substrates. J Magn Reson. 2012; 214:159–165. [PubMed: 22153915]
111. Adams RW, Duckett SB, Green RA, Williamson DC, Green GG. A theoretical basis for spontaneous polarization transfer in non-hydrogenative parahydrogen-induced polarization. J Chem Phys. 2009; 131:194505. [PubMed: 19929058]
112. Theis T, Ledbetter MP, Kervern G, Blanchard JW, Ganssle PJ, Butler MC, Shin HD, Budker D, Pines A. Zero-field NMR enhanced by parahydrogen in reversible exchange. J Am Chem Soc. 2012; 134:3987–3990. [PubMed: 22332806]
113. Walker TG, Happer W. Spin-exchange optical pumping of noble-gas nuclei. Rev Mod Phys. 1997; 69:629.
114. Goodson BM. Nuclear magnetic resonance of laser-polarized noble gases in molecules, materials, and organisms. J Magn Reson. 2002; 155:157–216. [PubMed: 12036331]
115. Nikolaou P, Coffey AM, Walkup LL, Gust BM, Whiting N, Newton H, Barcus S, Muradyan I, Dabaghyan M, Moroz GD, Rosen MS, Patz S, Barlow MJ, Chekmenev EY, Goodson BM. Near-unity nuclear polarization with an open-source 129Xe hyperpolarizer for NMR and MRI. Proc Natl Acad Sci USA. 2013; 110:14150–14155. [PubMed: 23946420]
116. Whiting N, Nikolaou P, Eschmann NA, Goodson BM, Barlow MJ. Interdependence of in-cell xenon density and temperature during Rb/129Xe spin-exchange optical pumping using VHG-narrowed laser diode arrays. J Magn Reson. 2011; 208:298–304. [PubMed: 21185208]
117. Walker, TG. Journal of Physics: Conference Series. IOP Publishing; 2011. Fundamentals of spin-exchange optical pumping; p. 012001
118. Rosen MS, Chupp TE, Coulter KP, Welsh RC, Swanson SD. Polarized 129Xe optical pumping/spin exchange and delivery system for magnetic resonance spectroscopy and imaging studies. Rev Sci Instrum. 1999; 70:1546–1552.
119. Oros AM, Shah NJ. Hyperpolarized xenon in NMR and MRI. Phys Med Biol. 2004; 49:R105. [PubMed: 15566166]
120. Schr der L. Xenon for NMR biosensing - inert but alert. Physica Med. 2013; 29:3–16.

121. Schröder L, Meldrum T, Smith M, Lowery TJ, Wemmer DE, Pines A. Temperature response of 129Xe depolarization transfer and its application for ultrasensitive NMR detection. Phys Rev Lett. 2008; 100:257603. [PubMed: 18643704]
122. Song YQ. Spin polarization-induced nuclear Overhauser effect: an application of spin-polarized xenon and helium. Concepts Magn Reson. 2000; 12:6–20.
123. Cherubini A, Bifone A. Hyperpolarised xenon in biology. Prog Nucl Magn Reson Spectrosc. 2003; 42:1–30.
124. Brunner E. Enhancement of surface and biological magnetic resonance using laser-polarized noble gases. Concepts Magn Reson. 1999; 11:313–335.
125. Navon G, Song Y-Q, Rõõm T, Appelt S, Taylor RE, Pines A. Enhancement of solution NMR and MRI with laser-polarized xenon. Science. 1996; 271:1848–1851.
126. Desvaux H, Dubois L, Huber G, Quillin ML, Berthault P, Matthews BW. Dynamics of xenon binding inside the hydrophobic cavity of pseudo-wild-type bacteriophage T4 lysozyme explored through xenon-based NMR spectroscopy. J Am Chem Soc. 2005; 127:11676–11683. [PubMed: 16104744]
127. Berthault P, Huber G, Ha PT, Dubois L, Desvaux H, Guittet E. Study of the hydrophobic cavity of β-cryptogein through laser-polarized xenon NMR spectroscopy. Chem Bio Chem. 2006; 7:59–64.
128. Spence MM, Rubin SM, Dimitrov IE, Ruiz EJ, Wemmer DE, Pines A, Yao SQ, Tian F, Schultz PG. Functionalized xenon as a biosensor. Proc Natl Acad Sci USA. 2001; 98:10654–10657. [PubMed: 11535830]
129. Berthault P, Huber G, Desvaux H. Biosensing using laser-polarized xenon NMR/MRI. Prog Nucl Magn Reson Spectrosc. 2009; 55:35–60.
130. Schröder L, Lowery TJ, Hilty C, Wemmer DE, Pines A. Molecular imaging using a targeted magnetic resonance hyperpolarized biosensor. Science. 2006; 314:446–449. [PubMed: 17053143]
131. Stevens TK, Ramirez RM, Pines A. Nanoemulsion contrast agents with sub-picomolar sensitivity for xenon NMR. J Am Chem Soc. 2013
132. Kazimierczuk K, Stanek J, Zawadzka-Kazimierczuk A, KoŸmiński W. Random sampling in multidimensional NMR spectroscopy. Prog Nucl Magn Reson Spectrosc. 2008; 57:420–434. [PubMed: 20920758]
133. Kupče Ē, Freeman R. Projection-reconstruction technique for speeding up multidimensional NMR spectroscopy. J Am Chem Soc. 2004; 126:6429–6440. [PubMed: 15149240]
134. Cornilescu G, Bahrami A, Tonelli M, Markley JL, Eghbalnia HR. HIFI-C: a robust and fast method for determining NMR couplings from adaptive 3D to 2D projections. J Biomol NMR. 2007; 38:341–351. [PubMed: 17610130]
135. Hyberts SG, Takeuchi K, Wagner G. Poisson-gap sampling and forward maximum entropy reconstruction for enhancing the resolution and sensitivity of protein NMR data. J Am Chem Soc. 2010; 132:2145–2147. [PubMed: 20121194]
136. Lescop E, Schanda P, Rasia R, Brutscher B. Automated spectral compression for fast multidimensional NMR and increased time resolution in real-time NMR spectroscopy. J Am Chem Soc. 2007; 129:2756–2757. [PubMed: 17305345]
137. Kupče Ē, Freeman R. Two-dimensional Hadamard spectroscopy. J Magn Reson. 2003; 162:300–310. [PubMed: 12810013]
138. Coggins BE, Venters RA, Zhou P. Radial sampling for fast NMR: concepts and practices over three decades. Prog Nucl Magn Reson Spectrosc. 2010; 57:381–419. [PubMed: 20920757]
139. Felli IC, Brutscher B. Recent advances in solution NMR: fast methods and heteronuclear direct detection. Chemphyschem. 2009; 10:1356–1368. [PubMed: 19462391]
140. Frydman L, Scherf T, Lupulescu A. The acquisition of multidimensional NMR spectra within a single scan. Proc Natl Acad Sci USA. 2002; 99:15858–15862. [PubMed: 12461169]
141. Gal M, Mishkovsky M, Frydman L. Real-time monitoring of chemical transformations by ultrafast 2D NMR spectroscopy. J Am Chem Soc. 2006; 128:951–956. [PubMed: 16417386]
142. Frydman L, Blazina D. Ultrafast two-dimensional nuclear magnetic resonance spectroscopy of hyperpolarized solutions. Nature Phys. 2007; 3:415–419.

143. Haupt J. A new effect of dynamic polarization in a solid obtained by rapid change of temperature. Phys Lett A. 1972; 38:389–390.

144. Sofikitis D, Rubio-Lago L, Martin MR, Brown DJA, Bartlett NCM, Alexander AJ, Zare RN, Rakitzis TP. Optical control of ground-state atomic orbital alignment: Cl (P) atoms from HCl (v= 2, J= 1) photodissociation. J Chem Phys. 2007; 127:144307. [PubMed: 17935395]

145. Van Kesteren H, Wenckebach WT, Schmidt J. Production of high, long-lasting, dynamic proton polarization by way of photoexcited triplet states. Phys Rev Lett. 1985; 55:1642. [PubMed: 10031877]

146. Kominis I, Kornack T, Allred J, Romalis M. A subfemtotesla multichannel atomic magnetometer. Nature. 2003; 422:596–599. [PubMed: 12686995]

147. Budker D, Romalis M. Optical magnetometry. Nature Phys. 2007; 3:227–234.

148. Greenberg YS. Application of superconducting quantum interference devices to nuclear magnetic resonance. Rev Mod Phys. 1998; 70:175–222.

149. McDermott R, Trabesinger AH, Mück M, Hahn EL, Pines A, Clarke J. Liquid-state NMR and scalar couplings in microtesla magnetic fields. Science. 2002; 295:2247–2249. [PubMed: 11910105]

150. Savukov I, Lee SK, Romalis M. Optical detection of liquid-state NMR. Nature. 2006; 442:1021–1024. [PubMed: 16943834]

151. Moulé AJ, Spence MM, Han SI, Seeley JA, Pierce KL, Saxena S, Pines A. Amplification of xenon NMR and MRI by remote detection. Proc Natl Acad Sci USA. 2003; 100:9122–9127. [PubMed: 12876195]

152. Poggio M, Degen C. Force-detected nuclear magnetic resonance: recent advances and future challenges. Nanotechnology. 2010; 21:342001. [PubMed: 20671365]

153. Köhler J, Disselhorst J, Donckers M, Groenen E, Schmidt J, Moerner W. Magnetic resonance of a single molecular spin. Nature. 1993; 363:242–244.

154. Wrachtrup J, Von Borczyskowski C, Bernard J, Orritt M, Brown R. Optical detection of magnetic resonance in a single molecule. Nature. 1993; 363:244–245.

155. Pietraiβ T, Gaede HC. Optically Polarized 129Xe in NMR Spectroscopy. Adv Mater. 1995; 7:826–838.

Highlights

- We discuss recent developments and emerging techniques to increase NMR sensitivity in liquids.
- General concepts underlying the determinants of NMR sensitivity and polarization enhancement are discussed.
- Main approaches covered: Fast NMR, dissolution DNP, Overhauser DNP, PHIP, spin- exchange optical pumping, photo-CIDNP.

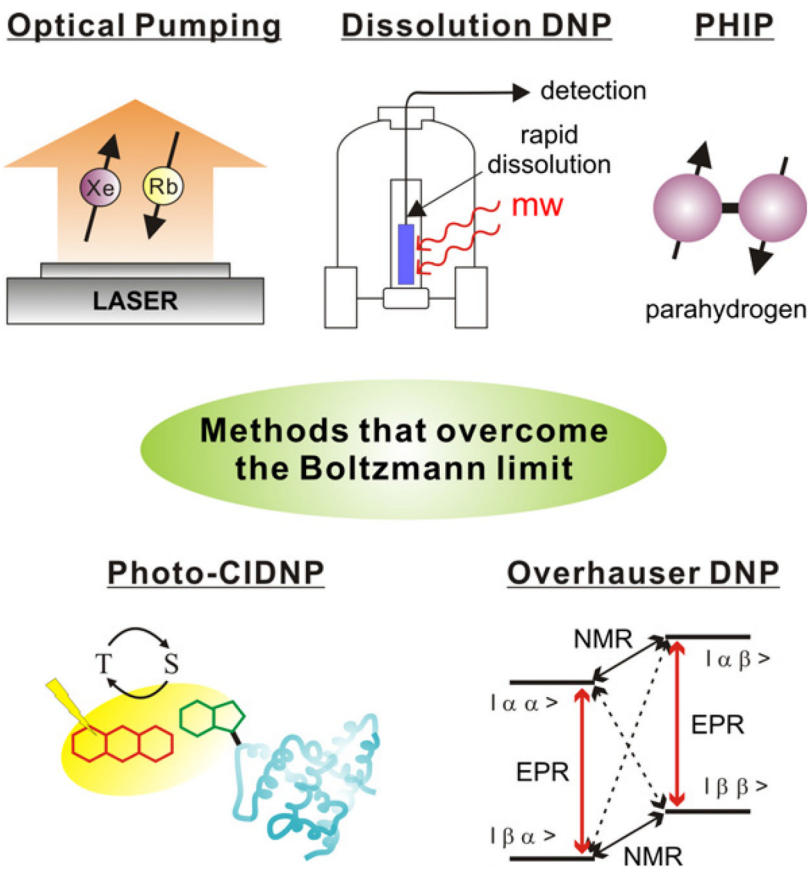

Fig. 1.
Overview of methods that perturb the longitudinal magnetization of nuclear spins in solution.

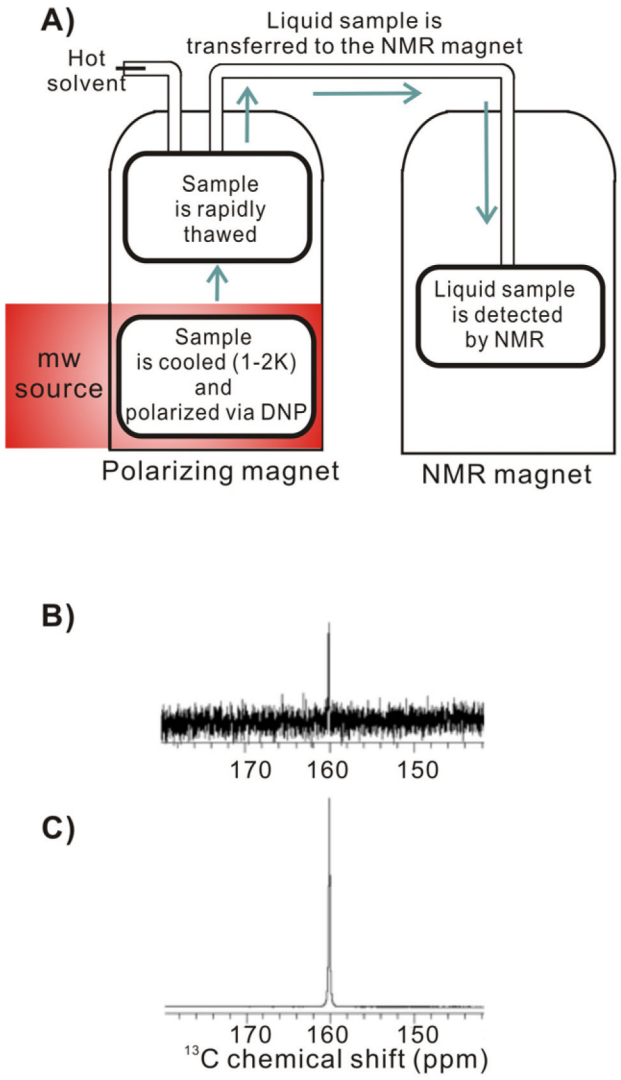

Fig. 2.

A) Schematic diagram illustrating the basic features of a dissolution DNP experiment. After hyperpolarization at low temperature by microwave (mw) irradiation, the sample is rapidly thawed and transferred to an NMR magnet for detection. B) Reference ^{13}C NMR spectrum of liquid urea (natural isotopic abundance, 59.6 mM, 232,128 scans) with no prior hyperpolarization and data collection under Ernst-angle conditions. C) ^{13}C NMR spectrum of liquid hyperpolarized urea (natural isotopic abundance, final concentration 59.6 mM, 1 scan) obtained via dissolution DNP in a 9.4T NMR magnet with final $P_{\%13C}$ = 20%. (Panels B and C were reprinted from Ref [37].)

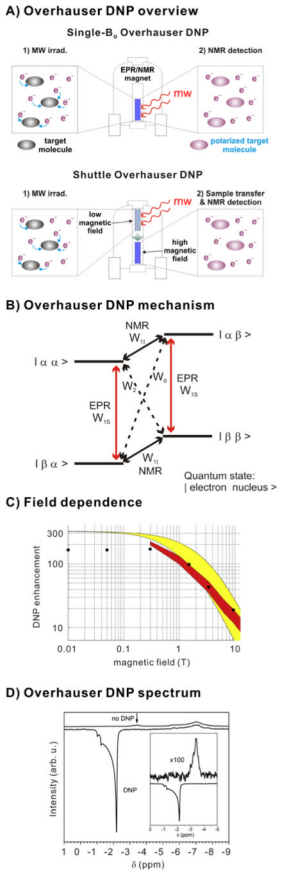

Fig. 3.

Schematic representation of the main aspects of Overhauser DNP. A) Single-B_0 and shuttle Overhauser DNP methods. B) Energy level diagram illustrating the Overhauser DNP mechanism. EPR transitions are saturated (red-double-headed arrows), causing an increase in double (W_2) and zero (W_0) quantum relaxation rates and an enhanced nuclear polarization. W_{1S} and W_{1I} denote single quantum transitions for electrons and nuclei, respectively. C) Experimental and predicted magnetic field dependence of Overhauser DNP enhancement of water relative to an unpolarized sample [66, 67]. Experimental DNP data are denoted as black dots. The theoretical field dependence of the coupling factor (assuming leakage and saturation factors to be 1) based on a force-free model is shown in yellow. MD simulations are shown in red. (Reprinted from Ref [67].) D) ^{1}H Overhauser DNP spectrum of water following high-power 260 GHz microwave irradiation at 9.2 T, leading to a >80-fold polarization enhancement relative to a nonpolarized control, corresponding to an Overhauser enhancement of −83 [71]. The change in chemical shift is due to sample heating. (Reprinted from Ref [71].)

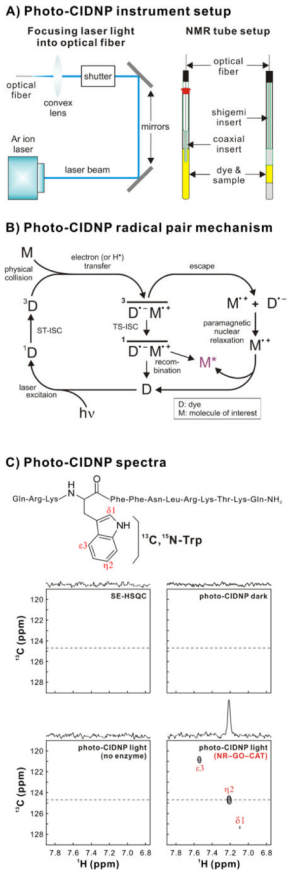

Fig. 4.

Overview of photo-CIDNP. A) Instrumental setup. B) Radical pair mechanism of photo-CIDNP in liquids. M* denotes the spin-polarized molecule of interest. C) 2D ^{13}C-PRINT photo-CIDNP spectra of the σ^{32} peptide (13-amino acids, 20 μM, 600 MHz spectrometer) in the absence and presence of catalytic amounts of the photo-CIDNP-enhancing NR-GO-CAT tri-enzyme system [95]. (Reprinted from [95].)

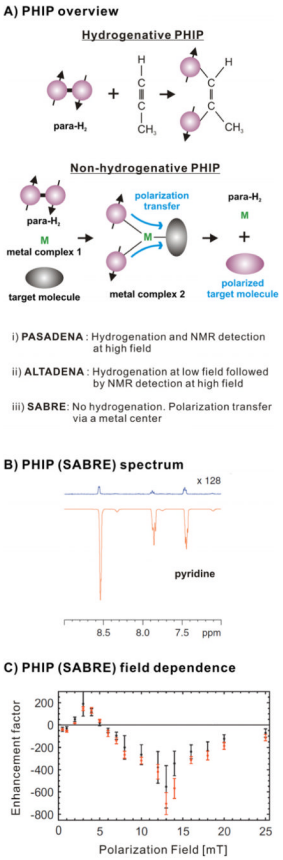

Fig. 5.

Schematic representation of PHIP. A) Overall mechanistic schemes for hydrogenative and non-hydrogenative PHIP. B) Non-hyperpolarized control (top) and SABRE-polarized (bottom) ^{1}H spectra of 6 nanomoles of pyridine [107]. The top spectrum is a 128-fold vertical expansion of the bottom spectrum. (Reprinted from [107].) C) Magnetic-field dependence of the SABRE PHIP enhancement factor for the proton linked to the pyridine C_4. Black and red dots denote regular pyridine and a 10:1 mixture of deuterated/protonated pyridine, respectively. Enhancement factors denote the ratio between the polarized and unpolarized signals. (Reprinted from [110].)

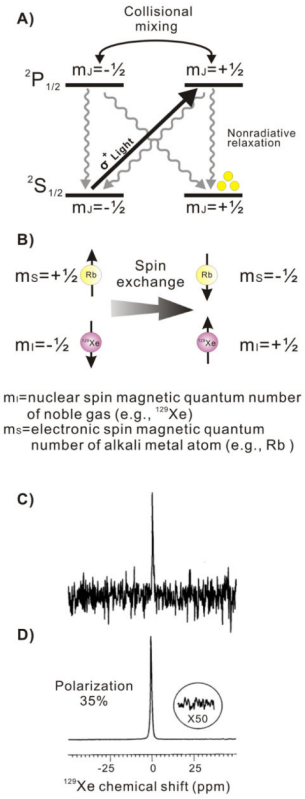

Fig. 6.

Overview of Optical pumping. A) Scheme illustrating the optical pumping of an alkali metal upon irradiation with right circularly polarized σ^+ light (the hyperfine coupling between electronic and nuclear spins is ignored). The process leads to an enriched population of the alkali metal in the $m_J = +1/2$ ground electronic state (yellow circles). B) Polarization transfer via spin exchange between the electron spin of an alkali-metal atom (e.g. Rb) and the nuclear spin of a noble gas (e.g. ^{129}Xe). C) Reference 1D ^{129}Xe NMR spectrum of 5×10^{19} gaseous Xe atoms in the absence of optical pumping. D) 1D ^{129}Xe NMR spectrum of 2×10^{17}gaseous Xe atoms (1 scan) polarized by optical pumping ($P_{\%,129Xe} = 37\%$). (Panels C and D were reprinted from [155].)

Table 1

Method	Absolute value of percent polarization $P_{\%}$	Advantages	Disadvantages
Optical Pumping	up to 90%[a] (^{129}Xe) [115, 118]	• High ^{129}Xe polarization values • ^{129}Xe is chemically inert and very sensitive to chemical environment • ^{129}Xe is soluble in water and biological fluids (e.g. liver, brain, blood) • Excellent tool as a biosensor to detect the presence of a target molecule	• Application to protein studies in solution is mostly limited to Xe-binding proteins or engineered biosensors due to the low solubility of ^{129}Xe in water • Detection is mostly limited to ^{129}Xe NMR • Direct detection of protein resonances by SPINOE is modest to date
Dissolution DNP	up to 40%[b] (^{13}C) [37, 51]	• High polarization can be achieved for low-γ nuclei • Several biologically relevant molecules and different nuclei have been tested	• Biomolecules often do not respond well to the fast thawing process • Significant sample dilution upon thawing • Usually only one polarization step is possible due to large dilution upon thawing • Long prepolarization times (min-hrs) are often necessary • Due to fast T_1 relaxation, only few transients can be acquired
Overhauser DNP	up to 0.26% (^{1}H) [71]	• Direct polarization in liquid phase • Useful to study water dynamics	• Lower enhancements at high field • Sample heating • Current applications are confined to water and small molecules
Photo-CIDNP	up to 0.23% (^{1}H, ^{15}N, ^{13}C, amino acids, peptides and proteins) [95] 4% (^{1}H, large photosynthetic reaction center) [98]	• Direct polarization in liquid phase • Applicable to free amino acids, peptides, proteins and nucleic acids • Wide range of sample concentration can be used (≥ 5μM) • Tri-enzyme additive prevents sample photodegradation and promotes dye recycling, supporting long-term data collection and 2D NMR • Observed enhancements increase with laser power • Very quick polarization buildup times (~ 0.1s)	• Relatively small enhancements • Only solvent-exposed aromatic amino acids undergo photo-CIDNP • Samples eventually degrade after very long exposure to high-power lasers
PHIP	~100% (^{1}H, hydrogenative PHIP) [105] ~11.5% (^{1}H, non-hydrogenative SABRE PHIP) [108]	• High polarization values • Effective at low sample concentrations (~ pmol) • SABRE approach can be applied to a variety of molecules	• SABRE works only at ~ mT magnetic fields • Current applications are mostly confined to small molecules

[a] Reported values refer to ^{129}Xe polarization achieved in the gas phase.

[b] Reported values refer to polarization achieved after transfer to the liquid phase.